LANGMUIR

Article

pubs.acs.org/Langmuir

Microstructure and Elastic Properties of Colloidal Gel Foams

Joseph T. Muth and Jennifer A. Lewis*

John A. Paulson School of Engineering and Applied Sciences, Wyss Institute for Biologically Inspired Engineering, Harvard University, Cambridge, Massachusetts 02138, United States

Supporting Information

ABSTRACT: Colloidal gel foams are composed of a continuous, attractive particle network that surrounds and interconnects dispersed bubbles. Here, we investigate their stability, morphology, and elasticity as a function of foaming intensity, surfactant concentration and hydrophobicity, pH, and colloid volume fraction. Upon optimizing these parameters, highly stable colloidal gel foams are created. Within this stability region, the specific interfacial area between the continuous (colloidal gel) and dispersed (bubble) phase can be varied over 2 orders of magnitude leading to a concomitant increase in storage modulus, which scales nearly linearly with specific interfacial area. Our observations provide design guidelines for attractive-particle stabilized foams that enable the programmable assembly of architected porous materials.

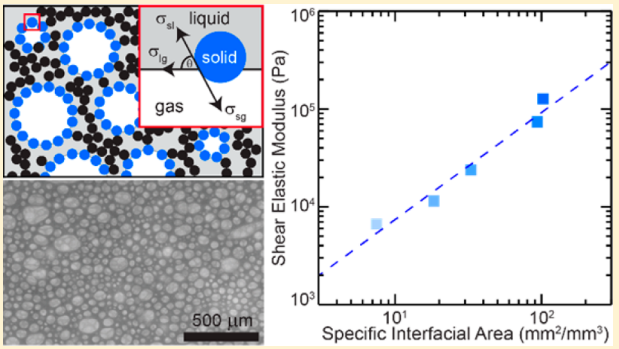

INTRODUCTION

Foams and emulsions are widely used in pharmaceuticals,[1] food,[2,3] cosmetics,[4] and, most recently, as inks for 3D printing of lightweight cellular architectures.[5,6] Their stability, structure, and rheological properties must be tailored for each targeted application of interest. Because of the large excess area associated with the liquid−gas (foam) or oil−water (emulsion) interfaces, such systems are inherently unstable and cream, coalesce, or disproportionate in the absence of sufficient interfacial stabilization. Colloidal particles, which irreversibly adsorb onto these interfaces, are known to impart long-term stability to both foams and emulsions, the latter of which are referred to as Pickering emulsions.[7−13] Particle stabilization is highly effective at preventing van der Waals collapse, retarding Ostwald ripening, and in some cases arresting gravitational syneresis.[7,10−12,14]

Interfacial stabilization arises when particles form an armor-like layer at the liquid−gas or oil−water interfaces.[15,16] If all particles in the system adsorb onto the interfaces, interfacial stabilization is possible for colloid volume fraction (ϕ_c) as low as approximately 0.0001−0.01, depending on the characteristic particle size and total interfacial area.[1] In this case, van der Waals collapse and Ostwald ripening are hindered by the interfacial particle layer.[11,12] For repulsive interparticle interactions, the microstructure and elasticity of these systems are qualitatively similar to surfactant stabilized foams and emulsions.[15,16] Namely, they possess negligible elasticity below random close packing of the dispersed phase ($\phi_{rcp} = 0.635$) and gel-like elasticity above ϕ_{rcp}.[17,18] Several scaling laws have been proposed for particle-free foams. In the limit where the volume fraction of the dispersed phase (ϕ_b) approaches unity (i.e., "dry" systems), Derjaguin,[19] and later Wilson,[20] showed that the foam storage modulus (G') scales as $G' \sim \sigma\Sigma$, where σ is the surface tension and Σ is the specific interfacial area (interfacial area per unit volume). In their analysis, the elasticity of the system is proportional to the surface tension in the polyhedral faces of the compressed foam cells and the amount of interfacial area in the system. Princen and Kiss,[17] and more recently Mason and Weitz,[18] described dispersed system elasticity over a broader ϕ_b range. Mason and Weitz showed $G' \sim \sigma\phi_b(\phi_b - \phi_{rcp})/r$, where r is the droplet radius.[18] Their result emphasizes that elasticity in repulsive dispersed systems scales with the Laplace pressure and arises when the system is compressed above close packing, allowing adjoining interfaces to transmit stress throughout the system. While particle-stabilized systems exhibit similar scaling to their particle-free counterparts, their elasticity scales with the elasticity of the interfacial stabilizing layer instead of the Laplace pressure.[4,15,16] Interfacial stabilization can also occur when there are excess repulsive particles dispersed in the continuous phase, beyond what is necessary for forming particle-adsorbed interfacial layers.[1,21] In this case, system stability is further enhanced due to the increased viscosity of the continuous phase, which retards fluid flow.

When attractive interactions are introduced between colloidal particles, the elasticity of the adsorbed particle layers increases and the dispersed phase may percolate for $\phi_b < \phi_{rcp}$.[16,22] In some cases, individual particles may bridge two interfaces, forming a Pickering emulsion gel.[23] As the attractive particle volume fraction increases beyond that required solely

Received: May 3, 2017
Revised: June 10, 2017

DOI: 10.1021/acs.langmuir.7b01476
Langmuir XXXX, XXX, XXX−XXX

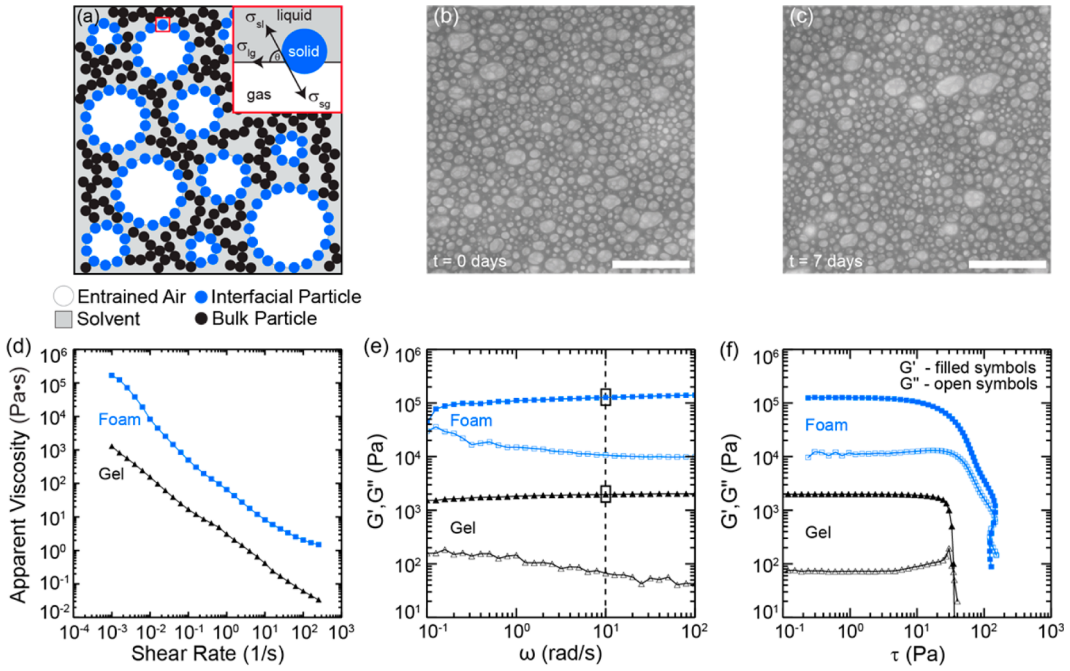

Figure 1. Stability, microstructure, and elasticity of colloidal gel foams (CGFs). (a) Scheme of CGF structure in which particle-stabilized bubbles are connected by the gel network of the continuous phase. Bubble stabilization is enabled by controlling the contact angle of the particles such that they spontaneously adsorb on the liquid−gas interface. Images of a representative CGF wet microstructure (b) immediately after foaming and (c) 1 week after foaming (scale bars: 500 μm). Bubble volume fraction (ϕ_b) and bubble size (d) are nearly identical between each image, indicating effective stabilization. Plots of (d) apparent viscosity as a function of shear rate as well as storage (G') and loss moduli (G'') (e) as a function of frequency (ω) and (f) shear stress (τ), for the representative precursor gel and its corresponding CGF. Reported storage moduli values are taken at ω = 10 rad/s.

for interfacial stabilization, excess particles within the continuous phase may form a space-filling particle network, i.e., a colloidal gel, provided $\phi_c > \phi_{gel}$,[24−28] further suppressing destabilization.[1,2,14,24,25] The addition of a dispersed phase (e.g., air or an immiscible liquid) to the continuous colloidal gel phase increases the elasticity of the system, where the bulk elasticity is now affected by the attractive particle network that surrounds the dispersed phase. The elastic properties of attractive-particle stabilized systems may be akin to attractive colloidal systems,[29−32] i.e., $G' \sim \phi_c^n$, except G' may depend on either ϕ_b[16,22] or ϕ_c[23,33] depending on the aggregation mechanism of the dispersed phase.

To date, most studies have focused on particle-stabilized systems in which the droplet/bubble volume fraction and stability are maximized, while retaining excellent flow properties.[12,13,16] These design criteria favor systems with repulsive or weakly attractive interparticle interactions and low ϕ_c.[13] However, recent efforts to develop particle-stabilized foams and emulsions for 3D printing of hierarchical porous materials underscore the need for systems with strongly attractive interparticle interactions and solids loading far above the limits where percolation theory describes colloidal gel behavior.[5,6] For example, we recently produced architected porous ceramics in the form of open honeycomb lattices composed of closed cell foam struts via direct foam writing.[5] Upon sintering, these hierarchical structures exhibited excellent mechanical properties, including high specific stiffness. However, the structure and elasticity of attractive-particle stabilized foams used to create such structures, which we refer to as colloidal gel foams, are poorly understood.[34,35]

In this paper, we investigate the stability, microstructure, and elasticity of colloidal gel foams (CGFs) created by mechanically frothing aqueous suspensions of attractive alumina particles of varying composition. Prior to foaming, the pure colloidal gels exhibit a solid-like response, with a frequency-independent storage modulus (G') that exceeds the loss modulus (G'') in the linear viscoelastic regime, fluid-like characteristics ($G' < G''$) at shear stresses (τ) exceeding a critical yield stress (τ_y), strong power law dependence of G' on ϕ_c,[36,37] and plateau modulus (G'_c) that is roughly 2 orders of magnitude lower than their foamed counterparts (G'_f) (Figure 1 and Figure S1). By controlling the foaming intensity, surfactant concentration and length, pH, and the colloid volume fraction of precursor gels, we produce stable CGFs with distinct microstructural and elastic characteristics. These foams exhibit similar rheological characteristics to their precursors, i.e., pure colloidal gels.[29−32,37] We determine the processing window for producing stable CGFs and show that foam elasticity scales linearly with the specific interfacial area between the continuous (gel) and dispersed (bubble) phases, rather than ϕ_c as expected for pure colloidal gels in the absence of dispersed bubbles.[29−32] Our results provide new insights into the structure−elasticity relationships of colloidal gel foams as well as processing guidelines for creating novel inks for additive manufacturing of hierarchically porous materials.

EXPERIMENTAL SECTION

Materials System. Colloidal gels and CGFs are produced by first suspending an appropriate amount of α-alumina particles (AKP 30; Sumitomo Chemical; mean diameter = 300 nm and Brunauer−Emmett−Teller surface area ~7.5 m^2/g) in deionized (DI) water at pH< 3 (adjusted by adding hydrochloric acid, HCl) to produce a well-dispersed colloidal suspension (ϕ_c = 0.51). This stock suspension is mixed in a planetary mixer (SpeedMixer DAC 600.2; FlackTek, Inc.) for 1 min at 800, 1200, and 1600 rpm and 7 min at 2000 rpm to disperse the alumina particles, followed by ball milling for at least 48 h using 5 mm yttria-stabilized zirconia spherical milling media in a 2:1

DOI: 10.1021/acs.langmuir.7b01476
Langmuir XXXX, XXX, XXX−XXX

mass ratio relative to the suspension. After milling, Λ, the desired amount of sodium X-sulfonate, where the number of alkane carbons (X) varies from 5 to 7 (i.e., sodium pentanesulfonate (X = 5), Sigma-Aldrich; sodium hexanesulfonate (X = 6), Sigma-Aldrich; sodium heptanesulfonate (X = 7), Alfa Aesar) is added per m^2 of colloid surface area to partially hydrophobize the alumina particles.[38] Colloidal gels are produced from this stock suspension by adjusting their final ϕ_c (0.25−0.45) and pH through the addition of DI water and either sodium hydroxide or nitric acid. After each addition, the suspension is mixed for 120 s at 2000 rpm. Once the desired solids loading and pH have been achieved, the resulting colloidal gel is characterized within 24 h.

To create the desired CGFs, 60 g of each representative colloidal gel is foamed in a 240 mL glass jar (SS CLR; VWR). Air is entrained using a four-bladed impeller (316L Cross Stirrer; Scilogex) and overhead mixer (OS20-S; Scilogex) at 400, 500, 750, 900, 1100, 1200, and 1500 rpm for 300 s each. Final foaming is performed with a flat-bottomed whisk (triangular 10.5 in. flat bottom whisk; Rattleware) at 1500 rpm for 90 s in the presence of an air stream (Movie S1). Foaming intensity levels are denoted by 25% (400 rpm), 50% (750 rpm), 75% (1100 rpm), 100% (1500 rpm), and 100W% (100% + whisk), where a given intensity level includes all lower intensities. All foams are characterized immediately after foaming unless otherwise stated. CGFs are defined as unstable, when any coarsening or drainage occurs within the first 24 h period. By contrast, the total bubble content and mean bubble size are retained in stable CGFs for at least 1 week (Figure 1b,c).

Microscopy and Image Analysis. The bubble volume fraction (ϕ_b) and diameter (d) are obtained for each foam by carrying out image analysis on micrographs acquired by transmission optical microscopy (VHX 2000, Keyence). Images are taken immediately after producing CGFs of varying composition. ϕ_b is obtained using the systematic point count method (ASTM E562-08). At least 420 grid points are analyzed over 12.2 mm^2 for each wet foam. d is obtained using the linear intercept method for two-phase materials (ASTM E112-13), where bubbles are defined as the dispersed phase and the alumina gel is defined as the continuous phase. At least 60 mm of lines are analyzed over 12.2 mm^2. To ensure equal interfacial area comparison between CGFs with different bubble content, interfacial area is reported per unit volume of foam and is calculated from ϕ_b and d according to $\Sigma = [(6\phi_b)/d] \times 1000$ where d is in μm, 1000 is a unit conversion from μm to mm, and Σ has units of mm^2/mm^3 or mm^{-1}.[39] Reported averages and standard deviations correspond to values obtained from at least three different images.

Contact Angle Measurements. These measurements are performed by depositing a 10 μL drop of the surfactant solution of interest onto an appropriately functionalized surface of a polished and cleaned α-alumina substrate (AKP 30; Sumitomo Chemical). The substrates are first cleaned by immersing them in a piranha solution (3:1 ratio of sulfuric acid (96% H_2SO_4) to hydrogen peroxide (30% H_2O_2)) followed by heating to 120 °C for at least 20 min. Each substrate is rinsed with DI water for at least 1 min, dried in flowing nitrogen, and then functionalized by immersion in an aqueous solution with controlled surfactant composition and pH. After immersion, the functionalized substrate is gently dried in flowing nitrogen. Contact angle measurements are acquired by depositing a droplet of that same surfactant solution onto the precleaned and functionalized alumina substrate. All reported values represent the average and standard deviation obtained from at least five separate measurements.

Rheometry. The rheological properties of the precursor colloidal gels and CGFs are characterized at 21 °C using a hybrid rheometer (Discovery HR-3 hybrid rheometer; TA Instruments). A 40 mm tapered cone geometry (2.005° 56 μm truncation gap) is used for the gels, while a custom-made 8-bladed vane (15 mm diameter, 38.5 mm height, 1.3 mm blade thickness, 4 mm gap) is used for the CGFs. A solvent trap is used for all tests to prevent solvent loss. Prior to testing, all gels are homogenized for 60 s at 2000 rpm and then carefully placed on the rheometer stage using a spatula. CGFs are tested immediately after frothing and loaded into the cup using a custom dispensing system to minimize differences in loading conditions between specimens. Prior to acquiring measurements, each sample is allowed to equilibrate for at least 15 min while undergoing low-amplitude oscillatory strain (γ) (γ = 0.001%, which is within the linear viscoelastic regime, Figure S2) or until G' varied negligibly over the experimental time scale. After equilibration, frequency sweeps are performed between 0.1 and 100 rad/s with strain amplitude of 0.001%. The values of G' for the CGF (G'_f) and precursor gel (G'_c) are taken at ω = 10 rad/s. Error bars correspond to G' at 1 rad/s (lower bound) and 100 rad/s (upper bound). Strain sweeps are performed from 5×10^{-4} to 100% strain at 1 Hz. The shear yield stress, τ_y, is defined by the crossover point where G'' exceeds G'. Flow sweeps are carried out between 0.001 and 250 s^{-1}.

RESULTS AND DISCUSSION

Colloidal gel foams of varying composition are produced by mechanically frothing aqueous suspensions of partially hydrophobized alumina particles (Movie S1). The particles spontaneously and irreversibly adsorb onto liquid−gas (bubble) interfaces introduced during foaming[7,9−12,40] (Figure 1a) when their attachment energy on the liquid−gas interface exceeds 10^3 kT, where k is the Boltzmann constant and T is absolute temperature.[11,41] The particle attachment energy (ΔE) is given by[11]

$$\Delta E = \pi r_p^{\,2} \sigma_{lg} (1 - \cos\theta)^2, \quad \theta < 90^\circ \tag{1}$$

where r_p is the particle radius, σ_{lg} is the liquid−gas interfacial energy, and θ is the contact angle. For the alkanesulfonate surfactants used in our work, σ_{lg} should range between 72.8 mN/m (i.e., pure water) and 40−50 mN/m (i.e., an alkane saturated water−gas interface).[11,42] Hence, a particle attachment energy of 10^3 kT (or higher) is calculated for our colloidal gel foams (r_p = 150 nm) when θ = 14°−90°.[11,41,42]

The adsorbed particles physically prevent the dispersed bubble phase from van der Waals collapse and Ostwald ripening and, for sufficiently attractive interparticle interactions, arrest drainage, yielding a stable foam microstructure that retains its characteristic bubble content and size over long times.[41] Direct imaging of wet foams stabilized by alumina particles (partially hydrophobized with Λ = 0.6 μmol/m^2 of X = 6, and a measured contact angle of 40 ± 11°) immediately after production (0 days) and aging (7 days) demonstrate that their ϕ_b (60.0 ± 3% and 59.0 ± 5%, respectively) and d (34.9 ± 2.7 μm and 33.9 ± 3.2 μm, respectively) remain nearly constant (Figures 1b,c).

The rheological properties of a representative precursor colloidal gel and CGF (Λ = 0.6 μmol/m^2 of X = 6, pH = 5, ϕ_c = 0.35) are shown in Figures 1d−f. Under these conditions, the colloidal particles are attractive, resulting in the formation of a colloidal gel that exhibits strong shear thinning behavior with an apparent viscosity ranging from ∼1000 Pa·s at 10^{-3} s^{-1} to ∼0.06 Pa·s at 10^2 s^{-1}. During mechanical foaming, the colloidal gel network is subjected to high shear rates that disrupt the attractive interparticle bonds, thereby allowing individual particles to adsorb onto the liquid−air interface during air entrainment. However, once foaming ceases, the attractive particle network quickly re-forms under quiescent conditions and surrounds each entrained air bubble. The plateau G'_c (∼2 × 10^3 Pa) and $\tau_{y,c}$ (∼30 Pa) of the colloidal gel network are sufficiently high to prevent syneresis. We find that syneresis does occur for CGFs created from colloidal gels with pH ≤ 4. Notably, after foaming the CGFs exhibit a sharp rise in their apparent viscosity, which increases by more than an order of magnitude over all shear rates investigated, along with a

DOI: 10.1021/acs.langmuir.7b01476
Langmuir XXXX, XXX, XXX−XXX

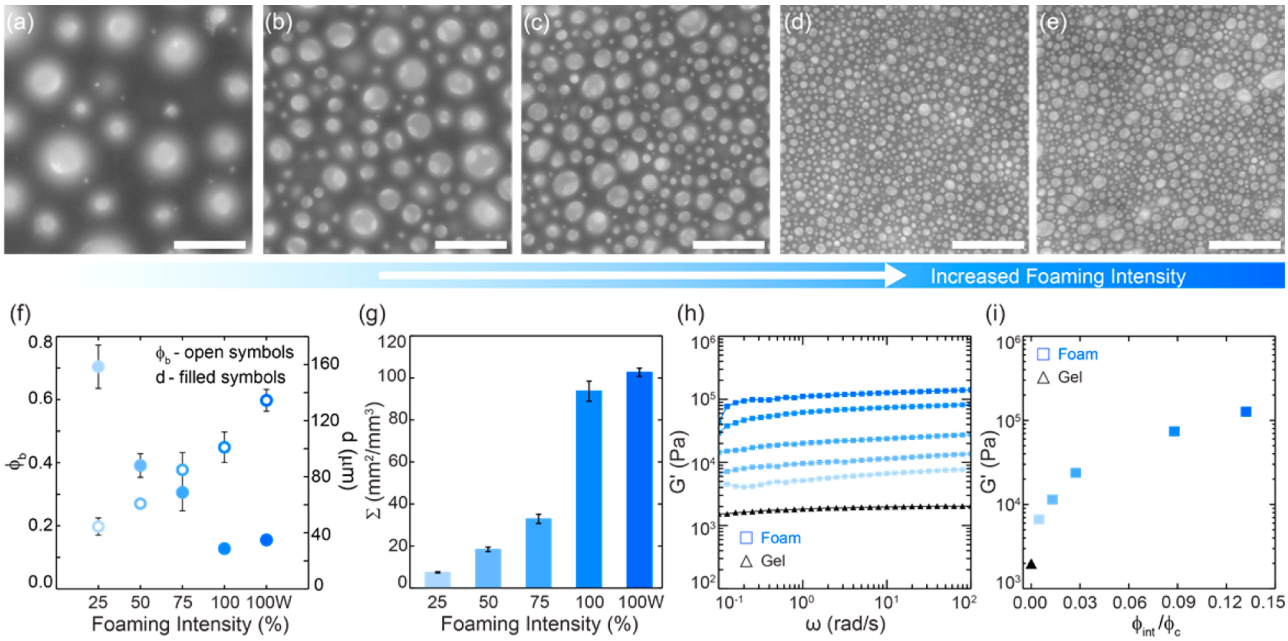

Figure 2. Foaming intensity effect on colloidal gel foam microstructure and elasticity. (a–e) Images of the CGF microstructure at 25%, 50%, 75%, 100%, and 100W% foaming intensity, respectively (scale bars: 500 μm). (f) Plots of bubble volume fraction (ϕ_b), bubble size (d), and (g) specific interfacial area (Σ) as a function of foaming intensity. Plots of storage modulus (G') as a function of (h) frequency (ω) and (i) normalized fraction of interfacially adsorbed particles (ϕ_{int}/ϕ_c), at the foaming intensities represented in (a–e) in the hexagonal limit for particle packing.

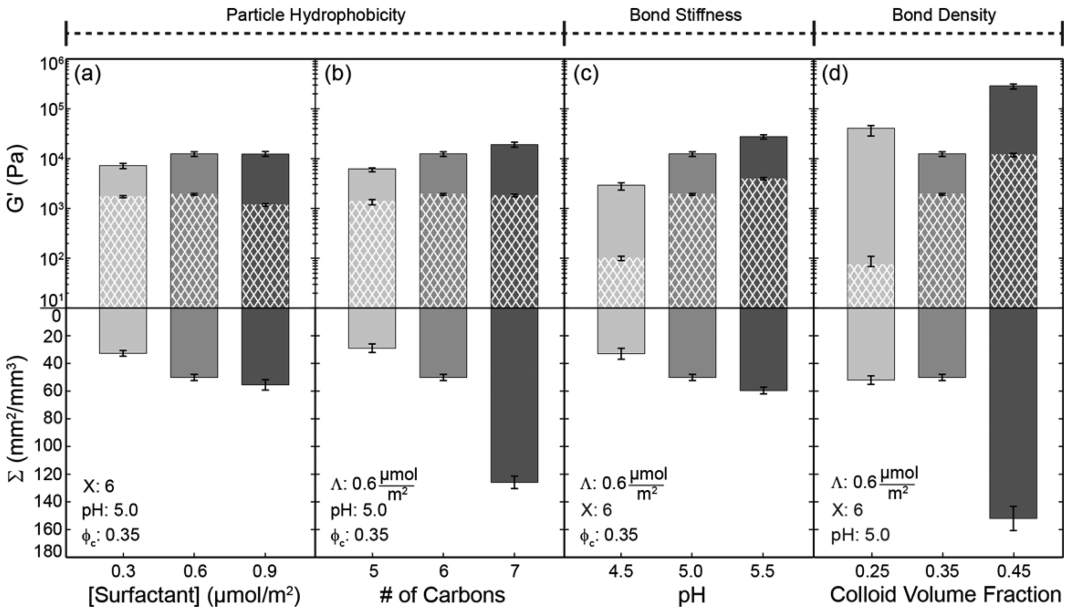

Figure 3. Storage modulus (G') and specific interfacial area (Σ) as a function of (a) surfactant concentration, (b) surfactant length, (c) pH, and (d) solids loading (ϕ_c). Bars represent the values for colloidal gel foams (solid) and colloidal gels (hatched).

concomitant increase in the plateau G'_f (~10^5 Pa) and $\tau_{y,f}$ (~10^2 Pa).

Next, we investigate the effects of mechanical foaming intensity on the structure and elasticity of this representative CGF (Λ = 0.6 μmol/m^2 of X = 6, pH = 5, ϕ_c = 0.35) (Figure 2). As foaming intensity increases from 25% to 100W%, ϕ_b increases from 0.20 to 0.60, while d decreases from 158 to 35 μm (Figure 2f). The foaming process leads to a concomitant rise in Σ from 7.5 to 103 mm^2/mm^3 over the same intensity range (Figure 2g). Increasing foaming intensity also produces stiffer CGFs; i.e., G'_f increases by over an order of magnitude over the full foaming intensity range (6.7 × 10^3 Pa at 25% to 1.3 × 10^5 Pa at 100W%) (Figure 2h).

We hypothesize that the increased elastic response of CGFs relative to their precursor gels may be related to the fraction of particles adsorbed on bubble interfaces (ϕ_{int}). To estimate ϕ_{int}, we approximate each CGF structure as a monodisperse system of spherical bubbles with size d, where the midplane of each adsorbed colloidal particle of radius r_p resides on the bubble interface. Because the particle stabilization process is a spontaneous surface phenomenon and $r_p \ll d/2$ for our system, the packing of adsorbed colloids on the bubble interfaces is two-dimensional and should attain a maximum

DOI: 10.1021/acs.langmuir.7b01476
Langmuir XXXX, XXX, XXX–XXX

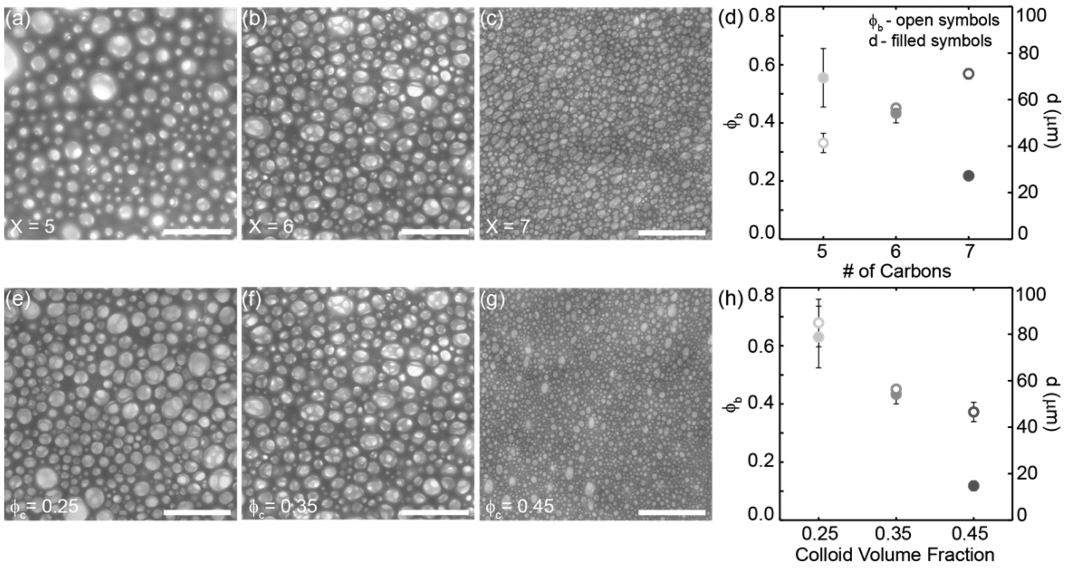

Figure 4. Surfactant alkane length (X) and colloid volume fraction (ϕ_c) effects on colloidal gel foam microstructure. (a–c) Images of CGFs with X = 5, 6, 7. (d) Plot of bubble volume fraction (ϕ_b) and bubble size (d) as a function of X. All CGFs described in (a–d) have Λ = 0.6 μmol/m^2, pH = 5.0, and ϕ_c = 0.35. (e–g) Images of CGFs with ϕ_c = 0.25, 0.35, and 0.45. (h) Plot of bubble volume fraction (ϕ_b) and bubble size (d) as a function of ϕ_c. All CGFs described in (e–h) have Λ = 0.6 μmol/m^2, X = 6, and pH = 5.0 [scale bars: 500 μm].

packing density near hexagonal close packing limit.[43−45] While perfect hexagonal packing (0.906) is not rigorously feasible in curved systems due to disclinations that form to accommodate bubble curvature,[44,46,47] we note that it serves as a useful upper limit for systems where $r_p \ll d/2$.[44,46,47] A more refined estimate of peak packing density may be used when r_p is similar to $d/2$.[43,44]

For a given CGF, it is straightforward to determine the volume of the continuous phase from ϕ_b, allowing ϕ_{int} to be calculated according to $\phi_{int} = (N_i V_p)/V_c$, where N_i is the total number of interfacial particles, V_p is the volume of an individual colloidal particle, and V_c is the total volume of the continuous phase. Figure 2i shows the evolution of G'_f with the normalized volume fraction of interfacial particles. At the lowest foaming intensity level, less than ∼0.5% of the particles within the CGF are adsorbed on the bubble interfaces, yet G'_f is 4-fold higher than that of the pure colloidal gel, G'_c. At the maximum foaming intensity, $\phi_{int}/\phi_c \sim 0.12–0.13$ and G'_f is nearly 2 orders of magnitude higher than G'_c. This dramatic increase in CGF stiffness may arise from the significant adsorption energies (∼10^3 kT or higher for 300 nm particles) associated with each particle adsorbed at the liquid–air interface.[11,41] This pinning energy is far higher than the estimated attractive interparticle bonds (∼few to 10s kT) between particles in the gel network.[30] Moreover, because the interfacial particles are more densely packed relative to the continuous gel phase,[48] they give rise to highly elastic, armor-like, layers that can dramatically affect bulk elasticity.[4,15,16] The observed rise in G'_f with increasing Σ (and therefore ϕ_{int}) occurs well below ϕ_{rcp}, since the continuous gel network within the CGF binds the interspersed bubbles together, effectively transmitting stress to the bubble interfaces through the backbone of interconnected particle clusters within the gel (Figure 1a). Similar trends are observed for all CGFs studied (Figure S3).

CGF structure and elasticity can be further manipulated by varying the composition of the colloidal (precursor) gel. The effects of each of these variables, Λ, X, pH, and ϕ_c, on CGF structure and elasticity are reported in Figures 3 and 4 (see also Figure S4 and Table S1), in which each CGF is subjected to maximum (100W%) foaming. Particle hydrophobicity is modified by varying the sodium hexanesulfonate (X = 6) concentration (Λ) from 0.3 to 0.9 μmol/m^2 and by changing alkane length from X = 5–7 at Λ = 0.6 μmol/m^2 (Figure 3a,b). We find that the contact angle for all values of Λ and X studied lies within the range of 35°–59° (Table S2). Importantly, G'_c is nearly constant over the entire range of surfactant concentrations and alkane lengths investigated; i.e., G'_c ranges from 1 × 10^3 to 2 × 10^3 Pa for pure colloidal gels, while G'_f ranges from 6 × 10^3 to 2 × 10^4 Pa for the CGFs.

As the surfactant hydrophobicity increases with longer alkane chain length, we observe a concomitant rise in particle hydrophobicity as reflected by our contact angle data, i.e., θ = 35 ± 2.5° for X = 5 and θ = 59 ± 5.0° for X = 7, which has a significant effect on the resulting CGF microstructure. The images provided in Figure 4 reveal that ϕ_b increases from 0.33 to 0.57 and d decreases from 69 to 27 μm as surfactant length increases from X = 5 to X = 7. Together, these changes are reflected by an increase in Σ from 29 to 126 mm^2/mm^3 for X = 5 and X = 7, respectively. The effects of Λ on particle hydrophobicity and CGF structure are minimal compared to the alkane chain length. θ, ϕ_b, d, and Σ range from 39 ± 11° to 44 ± 6°, 0.33 to 0.47, 61 to 51 μm, and 33 to 55 mm^2/mm^3, respectively, for Λ values between 0.3 and 0.9 μmol/m^2 (Figure S4).

Interparticle bond stiffness, reflected by G'_c, also affects CGF properties. As pH is varied from 4.5 to 5.5 (i.e., closer to the isoelectric point of alumina (pH ∼ 9), G'_c increases from 1.0 × 10^2 to 4.0 × 10^3 Pa. Over the same pH range, ϕ_b increases from 0.36 to 0.49, d decreases from 66 to 49 μm, and Σ increases from 33 to 60 mm^2/mm^3, respectively (Figure S4). We attribute the increase in Σ to changes in suspension stiffness, rather than changes in particle hydrophobicity, because less surfactant likely adsorbs onto the particles at higher pH values due to their lower positive charge. Higher pH values also correspond to stiffer CGFs (Figure 3c). G'_f increases by an order of magnitude from 2.9 × 10^3 Pa at pH 4.5 to 2.8 × 10^4 Pa

DOI: 10.1021/acs.langmuir.7b01476
Langmuir XXXX, XXX, XXX–XXX

at pH 5.5. Higher pH most likely fosters stronger interparticle attraction and increased flocculation in the continuous phase, while increased Σ promotes higher ϕ_{int} and additional interbubble bond formation. Both factors enhance the elasticity of CGF systems.[1,24,27,49]

The number density of attractive interparticle bonds scales with ϕ_c.[50] As ϕ_c increases from 0.25 to 0.45, G'_c increases dramatically from 7.6×10^1 to 1.2×10^4 Pa (Figure 3d). Interestingly, we find that systems with ϕ_c equal to 0.25 have nearly the same Σ and higher G'_f as systems with ϕ_c equal to 0.35, even though G'_c is 10× higher in the latter case. As Figure 4 illustrates, their similarity in Σ, values of 52 and 50 mm^2/mm^3, respectively, arises due to differences in bubble morphology. CGFs prepared from precursor gels composed of $\phi_c = 0.25$ possess higher bubble content ($\phi_b = 0.68$) and larger bubble size ($d = 79$ μm). By contrast, CGFs prepared from precursor gels with $\phi_c = 0.35$ possess fewer, but smaller, bubbles ($\phi_b = 0.45$, $d = 54$ μm). On the basis of these morphology differences, we hypothesize that the increased stiffness of CGFs with $\phi_c = 0.25$ compared to CGFs with $\phi_c = 0.35$ may stem from bubble interface distortion since $\phi_b > \phi_{rcp}$.[16] Other attractive dispersed systems near the close packing threshold also demonstrate stiffness increases relative to systems in which ϕ_b is much lower than close packing.[49] Note, however, that the random close packing fraction for polydisperse systems may be as high as 0.68.[51] The stiffest CGF arises from the most concentrated precursor gel, $\phi_c = 0.45$, explored. Because of its high G'_c, smaller bubbles ($d = 15$ μm) are incorporated, leading to the highest Σ and G'_f values of 152 mm^2/mm^3 and 2.9×10^5 Pa, respectively, despite having $\phi_b < 0.40$.

Our observations suggest that interfacial stabilization modestly affects the elasticity and microstructural evolution of these colloidal gel foams. For example, there is a 4-fold increase in Σ accompanied by a 3-fold increase in G'_f, when X increases from 5 to 7. By contrast, the particle network strongly affects the foam morphology and stiffness. Both pH (bond stiffness) and ϕ_c (bond density) increases lead to a pronounced increase in Σ, and the elasticity of CGFs increases over an order of magnitude over these experimental conditions.

While the microstructure and elasticity of CGFs are of primary interest, we also explored the stability of CGFs to understand the range of achievable properties. A stability map for CGFs prepared with $\phi_c = 0.35$, $\Lambda = 0.6$ μmol/m^2, and varying surfactant length, foaming intensity, and pH is shown in Figure 5a. Stable foams are obtained between pH 4.5 and 6.75 with Σ values ranging from 6 to 233 mm^2/mm^3 (Table S3). While bubbles could be entrained in precursor suspensions below pH 4.5, these foams are unstable and cream within 24 h. Within the stable region, the maximum Σ value at each pH starts at 152 mm^2/mm^3 at pH = 4.5, peaks at 233 mm^2/mm^3 at pH 5.5, and then decreases again to 136 mm^2/mm^3 at pH 6.75.

Our results suggest the stiffness of the gel network critically impacts CGF stability. The precursor gel must be robust enough to arrest bubble movement but not excessively stiff so to preclude aeration. During foaming, energy is supplied by the impeller (E_{mix}) to break apart particulate clusters within the precursor gel and introduce air within the CGF. When E_{mix} exceeds the energy required to introduce new interfacial area (E_{int}), aeration occurs. We hypothesize that stiffer gels and CGFs with higher Σ have higher E_{int} relative to less stiff gels and CGFs with lower Σ, since stiffer gels require more energy to rupture interparticle bonds, and higher Σ leads to more

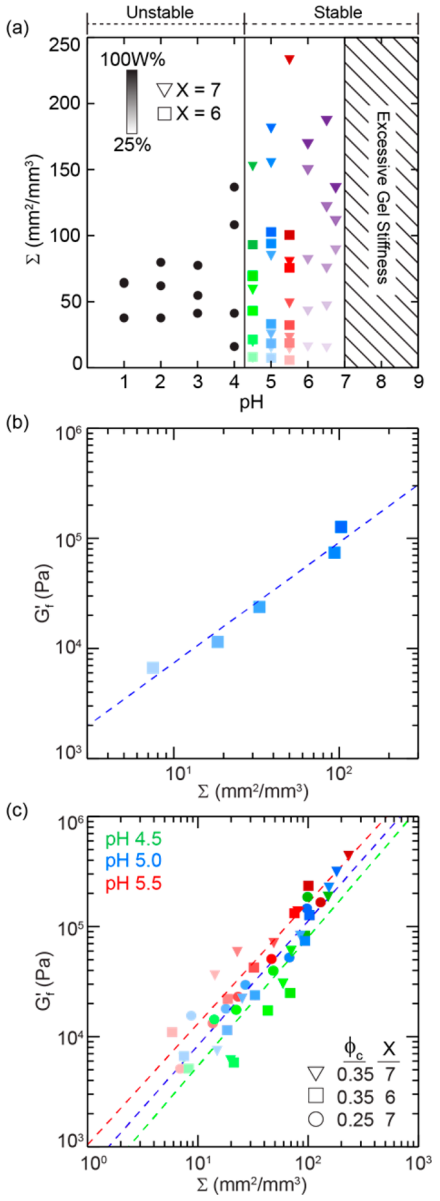

Figure 5. Stability and elastic properties of CGFs. (a) Map of specific interfacial area (Σ) and pH for CGFs formulated with colloid volume fraction (ϕ_c) = 0.35 and surfactant concentration (Λ) = 0.6 μmol/m^2 highlighting regions of stable and unstable CGFs. The hatched region would theoretically produce stable CGFs but is experimentally inaccessible due to excessive gel stiffness. Plots of storage modulus (G'_f) vs specific interfacial area (Σ) for (b) the representative CGF formulation and (c) CGFs at pH 4.5, 5.0, and 5.5 for various solids loadings (ϕ_c) and alkane chain length (X).

particles adsorbed in strong bonding states on the bubble interfaces.[1] Furthermore, E_{int} should increase progressively during foaming as ϕ_{int} increases. Aeration ceases when $E_{mix} < E_{int}$.

The presence of dispersed, yet unstable, bubbles at pH ≤ 4 ($G'_c \leq 3.3 \times 10^1$ Pa) indicates that sufficiently hydrophobic suspension conditions alone do not give rise to bulk foams, if the continuous phase is not stiff enough to resist creaming. Between pH 4.5 and 5.5, G'_c increases from 7.6×10^1 to 4.6×10^4 Pa and stable foams are formed. In this pH range, stiffer gels are capable of entraining smaller bubbles without compromising ϕ_b, leading to higher Σ (Figure S5). Note that

DOI: 10.1021/acs.langmuir.7b01476
Langmuir XXXX, XXX, XXX−XXX

ϕ_b is similar between pH 4.5 (ϕ_b = 0.56) and pH 5.5 (ϕ_b = 0.53), but foams prepared at pH 5.5 possess bubbles that are 40% smaller in size than those found at pH 4.5, i.e., d = 14 μm and d = 22 μm, respectively. Therefore, peak Σ for stable CGFs at pH < 5.5 is limited by G'_c since peak foaming intensity produces increasingly small bubbles at similar air content. However, as G'_c increases from 4.6 × 10^4 to 1.8 × 10^5 Pa between pH 5.5 and 6.75, a larger fraction of E_{mix} is devoted to separating particle flocs, causing a significant reduction in ϕ_b (pH 6.75: ϕ_b = 0.37) (Figure S5), yielding lower Σ. The upper pH bound for foam formation occurs at pH 6.75, where E_{int} of the gel alone exceeds E_{mix}, preventing foam formation. Thus, CGFs formulated at pH > 5.5 are limited by E_{mix}, although in principle stable foams should be accessible up to pH values approaching the IEP with sufficiently energetic aeration. It is expected that for ϕ_c < 0.35 the same stability trends would occur except the lower bound stability threshold pH would increase to compensate for lower interparticle bond density. Conversely, for ϕ_c > 0.35, stability should begin at lower pH, since bond density will be higher. For insufficiently hydrophobic particles, it is well-known that foaming will not occur regardless of network structure.[13,41] While particle hydrophobicity will also change as a function of pH, the physical phenomena (i.e., gravitational syneresis and interparticle bond energy) that govern the stability bounds in our system depend far more strongly on G'_c than particle hydrophobicity.

To evaluate the scaling of G'_f with Σ, we created CGFs from nine different precursor formulations with X = 6 or 7 and ϕ_c = 0.25 or 0.35 over a pH range between the onset of CGF stability (pH 4.5) and the pH value corresponding to the maximum realized Σ (pH 5.5). For each formulation, the surfactant concentration is fixed at 0.6 μmol/m^2, foaming intensity ranges between 25% and 100W%, and Σ and G'_f are measured at each foaming level. Results for the reference CGF are shown in Figure 5b. As foaming intensity increases, Σ and G'_f increase from 7.5 mm^2/mm^3 and 6.7 × 10^3 Pa at 25% to 103 mm^2/mm^3 and 1.3 × 10^5 Pa at 100W%. Plotting G'_f as a function of Σ reveals a linear dependence with a scaling exponent near unity (i.e., n = 1.09, r^2 = 0.96). Remarkably, similar scaling behavior is observed over a wide Σ range (Σ = 6−233 mm^2/mm^3) independent of X, ϕ_c, or pH (n_{avg} = 1.12 ± 0.18) (Figure S6 and Table S4). These results may be explained by the proposed CGF structure shown in Figure 1a. We hypothesize that the partially hydrophobized particles adsorb on the bubble interfaces, while the continuous gel phase percolates between bubbles. The elasticity of the system arises from the interconnected bubble-filled gel network. For a given CGF, we assume that (1) interfacial characteristics are governed by the precursor formulation, (2) all interfaces within a given system have the same elastic properties, (3) there exists a fixed number of bonds per unit interfacial area, and (4) new interfacial area has the same probability of participating in interbubble bonding, as previously incorporated interfacial area.[49] By increasing Σ at otherwise constant conditions, more particles will partition to entrained interfaces, and the connectivity of the bubble network will increase, leading to a concomitant rise in G'_f. In good agreement with this proposed structural model, we find that increasing Σ for a given foam formulation via foaming intensity yields a linearly proportional increase in elasticity, since every unit of interfacial area has the same properties and interacts with the continuous gel equivalently.

To compare the elasticity between foam formulations, one must account for differences in the interbubble bond stiffness. For systems with equivalent Σ, it is expected that the CGFs with stronger interparticle attractions will have stiffer interbubble bonds and therefore larger G'_f. We observe this behavior when G'_f and Σ are compared as a function of bond stiffness (i.e., pH) in Figure 5c. Namely, the same linear scaling observed for individual formulations persists for each bond stiffness level (pH 4.5: n = 1.17, r^2 = 0.81, pH 5: n = 1.13, r^2 = 0.92, pH 5.5: n = 1.10, r^2 = 0.92), but the pre-exponential factor c, which is related to the effective interbubble bond stiffness in our proposed microstructure−elasticity model, increases with increasing pH from 2.56 Pa·mm^n at pH 4.5 to 3.02 Pa·mm^n at pH 5.5 (Figure S7). These findings are similar to the results reported by Derjaguin and Wilson for dry foams.[19,20] However, the mechanism for stress transfer in dry foam systems (interfacial distortion) is replaced by attractive interparticle bridges that form between neighboring bubble interfaces in CGFs. When ϕ_b < ϕ_{rcp}, interbubble bonding and interfacially adsorbed particles most likely dominate their elastic response. Of course, additional interfacial contributions to foam stiffness would arise when ϕ_b > ϕ_{rcp}.

CONCLUSION

We have explored the stability, microstructure, and elasticity of colloidal gel foams characterized by high solids loading and attractive interparticle interactions. By manipulating particle hydrophobicity, interparticle bond stiffness and density, and foaming intensity, we created stable CGFs whose specific interfacial area and stiffness could be varied over 2 orders of magnitude. The boundary conditions for designing stable foams have been defined. Our observations suggest that CGF microstructures may be idealized as a network of particle stabilized bubbles interconnected by attractive particulate bridges that form within the continuous colloidal gel phase. Over all foam compositions studied, we found that the foam elasticity scales linearly with the specific area of the colloidal gel−bubble interface. Our observations provide processing guidelines to further advance the directed assembly of porous architectures derived from colloidal gel foams.

ASSOCIATED CONTENT

Supporting Information

The Supporting Information is available free of charge on the ACS Publications website at DOI: 10.1021/acs.langmuir.7b01476.

Elasticity data for pure colloidal gels (Figure S1); rheology data for precursor gels and foams showing the strain limits of the linear viscoelastic regime (Figure S2); foam elasticity as a function of the normalized volume fraction of particles adsorbed on bubble interfaces (Figure S3); microstructures of CGFs with various surfactant concentrations and suspension pH values (Figure S4); precursor gel elasticity and CGF microstructure data for selected formulations in Figure 5a (Figure S5); foam elasticity as a function of specific interfacial area for all foams in Figure 5c (Figure S6); c as a function of pH as determined from the regressions in Figure 5c (Figure S7); formulation, microstructure, and elasticity information for colloidal gels and CGFs in Figure 3 (Table S1); contact angle data for representative formulations (Table S2); stability, microstructure and

DOI: 10.1021/acs.langmuir.7b01476
Langmuir XXXX, XXX, XXX−XXX

elasticity values of representative formulations in Figure 5a (Table S3); data and fitting results for CGF formulations in Figure 5c and Figure S6 (Table S4) (PDF)

Movie S1: the foaming process used to produce colloidal gel foams (MPG)

AUTHOR INFORMATION

Corresponding Author

*(J.A.L.) E-mail jalewis@seas.harvard.edu.

ORCID

Jennifer A. Lewis: 0000-0002-0280-2774

Author Contributions

J.T.M. and J.A.L. designed research; J.T.M. performed research; J.T.M. and J.A.L. wrote the paper. All authors have given approval to the final version of the manuscript.

Notes

The authors declare the following competing financial interest(s): I have co-founded a company, Voxel8, which is focused on commercializing 3D printing of electronics and reactive materials for athletic footwear.

ACKNOWLEDGMENTS

We gratefully acknowledge support from the National Science Foundation Grant DMR-1305284 and the National Science Foundation Graduate Research Fellow Program (J.T.M.). J.A.L. acknowledges support from the Vannevar Bush Faculty Fellowship Program sponsored by the Basic Research Office of the Assistant Secretary of Defense for Research and Engineering and funded by the Office of Naval Research Grant N00014-16-1-2823 and the generous donation from the GETTY LAB. We also thank Michael Kreder (Aizenberg Lab) for assistance with contact angle measurements and Dr. Lori K. Sanders for imaging assistance.

REFERENCES

(1) Chevalier, Y.; Bolzinger, M. A. Emulsions Stabilized with Solid Nanoparticles: Pickering Emulsions. *Colloids Surf., A* **2013**, *439*, 23−34.

(2) Dickinson, E. Food Emulsions and Foams: Stabilization by Particles. *Curr. Opin. Colloid Interface Sci.* **2010**, *15* (1), 40−49.

(3) Dickinson, E. Use of Nanoparticles and Microparticles in the Formation and Stabilization of Food Emulsions. *Trends Food Sci. Technol.* **2012**, *24* (1), 4−12.

(4) Arditty, S.; Schmitt, V.; Giermanska-Kahn, J.; Leal-Calderon, F. Materials Based on Solid-Stabilized Emulsions. *J. Colloid Interface Sci.* **2004**, *275* (2), 659−664.

(5) Muth, J. T.; Dixon, P. G.; Woish, L.; Gibson, L. J.; Lewis, J. A. Architected Cellular Ceramics with Tailored Stiffness via Direct Foam Writing. *Proc. Natl. Acad. Sci. U. S. A.* **2017**, *114*, 1832.

(6) Minas, C.; Carnelli, D.; Tervoort, E.; Studart, A. R. 3D Printing of Emulsions and Foams into Hierarchical Porous Ceramics. *Adv. Mater.* **2016**, *28* (45), 9993−9999.

(7) Pickering, S. U. CXCVI. - Emulsions. *J. Chem. Soc., Trans.* **1907**, *91*, 2001−2021.

(8) Ramsden, W. Separation of Solids in the Surface-Layers of Solutions and "Suspensions" (Observations on Surface-Membranes, Bubbles, Emulsions, and Mechanical Coagulation). – Preliminary Account. *Proc. R. Soc. London* **1903**, *72*, 156−164.

(9) Finkle, P.; Draper, H. D.; Hildebrand, J. H. The Theorgy of Emulsification. *J. Am. Chem. Soc.* **1923**, *45*, 2780−2788.

(10) Leja, J.; Schulman, J. H. Control of Contact Angles at the Oil-Water-Solid Interfaces. Emulsions Stabilized by Solid Particles ($BaSO_4$). *Trans. Faraday Soc.* **1954**, *50*, 598−605.

(11) Binks, B. P. Particles as Surfactants - Similarities and Differences. *Curr. Opin. Colloid Interface Sci.* **2002**, *7* (1−2), 21−41.

(12) Aveyard, R.; Binks, B. P.; Clint, J. H. Emulsions Stabilised Solely by Colloidal Particles. *Adv. Colloid Interface Sci.* **2003**, *100−102* (SUPPL), 503−546.

(13) Akartuna, I.; Studart, A. R.; Tervoort, E.; Gonzenbach, U. T.; Gauckler, L. J. Stabilization of Oil-in-Water Emulsions by Colloidal Particles Modified with Short Amphiphiles. *Langmuir* **2008**, *24* (14), 7161−7168.

(14) Alison, L.; Rühs, P. A.; Tervoort, E.; Teleki, A.; Zanini, M.; Isa, L.; Studart, A. R. Pickering and Network Stabilization of Biocompatible Emulsions Using Chitosan-Modified Silica Nanoparticles. *Langmuir* **2016**, *32* (50), 13446−13457.

(15) Bressy, L.; Hébraud, P.; Schmitt, V.; Bibette, J. Rheology of Emulsions Stabilized by Solid Interfaces. *Langmuir* **2003**, *19* (3), 598−604.

(16) Arditty, S.; Schmitt, V.; Lequeux, F.; Leal-Calderon, F. Interfacial Properties in Solid-Stabilized Emulsions. *Eur. Phys. J. B* **2005**, *44* (3), 381−393.

(17) Princen, H.; Kiss, A. Rheology of Foams and Highly Concentrated Emulsions: III. Static Shear Modulus. *J. Colloid Interface Sci.* **1986**, *112* (2), 427−437.

(18) Mason, T. G.; Bibette, J.; Weitz, D. A. Elasticity of Compressed Emulsions. *Phys. Rev. Lett.* **1995**, *75* (10), 2051−2054.

(19) Derjaguin, V. B. Die Elastischen Eigenschaften Der Schiiume. *Colloid Polym. Sci.* **1933**, *64* (7), 1−6.

(20) Stamenovic, D.; Wilson, T. A. The Shear Modulus of Liquid Foams. *J. Appl. Mech.* **1984**, *51*, 229−231.

(21) Hunter, T. N.; Pugh, R. J.; Franks, G. V.; Jameson, G. J. The Role of Particles in Stabilising Foams and Emulsions. *Adv. Colloid Interface Sci.* **2008**, *137* (2), 57−81.

(22) Leal-Calderon, F.; Schmitt, V. Solid-Stabilized Emulsions. *Curr. Opin. Colloid Interface Sci.* **2008**, *13* (4), 217−227.

(23) Lee, M. N.; Chan, H. K.; Mohraz, A. Characteristics of Pickering Emulsion Gels Formed by Droplet Bridging. *Langmuir* **2012**, *28* (6), 3085−3091.

(24) Katepalli, H.; John, V. T.; Tripathi, A.; Bose, A. Microstructure and Rheology of Particle Stabilized Emulsions: Effects of Particle Shape and Inter-Particle Interactions. *J. Colloid Interface Sci.* **2017**, *485* (2017), 11−17.

(25) Tzoumaki, M. V.; Moschakis, T.; Kiosseoglou, V.; Biliaderis, C. G. Oil-in-Water Emulsions Stabilized by Chitin Nanocrystal Particles. *Food Hydrocolloids* **2011**, *25* (6), 1521−1529.

(26) Simon, S.; Theiler, S.; Knudsen, A.; Øye, G.; Sjöblom, J. Rheological Properties of Particle-Stabilized Emulsions. *J. Dispersion Sci. Technol.* **2010**, *31* (5), 632−640.

(27) Abend, S.; Bonnke, N.; Gutschner, U.; Lagaly, G. Stabilization of Emulsions by Heterocoagulation of Clay Minerals and Layered Double Hydroxides. *Colloid Polym. Sci.* **1998**, *276* (8), 730−737.

(28) Thieme, J.; Abend, S.; Lagaly, G. Aggregation in Pickering Emulsions. *Colloid Polym. Sci.* **1999**, *277* (2−3), 257−260.

(29) Shih, W. H.; Shih, W. Y.; Kim, S. I.; Aksay, I. A. Scaling Behavior of the Elastic Properties of Colloidal Gels. *Phys. Rev. A: At., Mol., Opt. Phys.* **1990**, *42* (8), 4772−4779.

(30) Rueb, C. J.; Zukoski, C. F. Viscoelastic Properties of Colloidal Gels. *J. Rheol. (Melville, NY, U. S.)* **1997**, *41* (1997), 197−218.

(31) Grant, M. C.; Russel, W. B. Volume-Fraction Dependence of Elastic Moduli and Transition Temperatures for Colloidal Silica Gels. *Phys. Rev. E: Stat. Phys., Plasmas, Fluids, Relat. Interdiscip. Top.* **1993**, *47* (4), 2606−2614.

(32) Buscall, R.; Mills, P. D. A.; Goodwin, J. W.; Lawson, D. W. Scaling Behavior of the Rheology of Aggregate Networks Formed from Colloidal Particles. *J. Chem. Soc., Faraday Trans. 1* **1988**, *84* (12), 4249−4260.

(33) Kaganyuk, M.; Mohraz, A. Non-Monotonic Dependence of Pickering Emulsion Gel Rheology on Particle Volume Fraction. *Soft Matter* **2017**, *13* (13), 2513−2522.

DOI: 10.1021/acs.langmuir.7b01476
Langmuir XXXX, XXX, XXX−XXX

(34) Gonzenbach, U. T.; Studart, A. R.; Tervoort, E.; Gauckler, L. J. Tailoring the Microstructure of Particle-Stabilized Wet Foams. *Langmuir* **2007**, *23* (3), 1025−1032.
(35) Akartuna, I.; Studart, A. R.; Tervoort, E.; Gauckler, L. J. Macroporous Ceramics from Particle-Stabilized Emulsions. *Adv. Mater.* **2008**, *20* (24), 4714−4718.
(36) Conrad, J. C.; Lewis, J. A. Structure of Colloidal Gels during Microchannel Flow. *Langmuir* **2008**, *24* (15), 7628−7634.
(37) Conrad, J. C.; Ferreira, S. R.; Yoshikawa, J.; Shepherd, R. F.; Ahn, B. Y.; Lewis, J. A. Designing Colloidal Suspensions for Directed Materials Assembly. *Curr. Opin. Colloid Interface Sci.* **2011**, *16* (1), 71−79.
(38) Chuanuwatanakul, C.; Tallon, C.; Dunstan, D. E.; Franks, G. V. Controlling the Microstructure of Ceramic Particle Stabilized Foams: Influence of Contact Angle and Particle Aggregation. *Soft Matter* **2011**, *7* (24), 11464−11474.
(39) Frelichowska, J.; Bolzinger, M. A.; Chevalier, Y. Effects of Solid Particle Content on Properties of O/w Pickering Emulsions. *J. Colloid Interface Sci.* **2010**, *351* (2), 348−356.
(40) Gonzenbach, U. T.; Studart, A. R.; Steinlin, D.; Tervoort, E.; Gauckler, L. J. Processing of Particle-Stabilized Wet Foams into Porous Ceramics. *J. Am. Ceram. Soc.* **2007**, *90* (11), 3407−3414.
(41) Studart, A. R.; Gonzenbach, U. T.; Tervoort, E.; Gauckler, L. J. Processing Routes to Macroporous Ceramics: A Review. *J. Am. Ceram. Soc.* **2006**, *89* (6), 1771−1789.
(42) Megias-Alguacil, D.; Tervoort, E.; Cattin, C.; Gauckler, L. J. Contact Angle and Adsorption Behavior of Carboxylic Acids on α-Al2O3 Surfaces. *J. Colloid Interface Sci.* **2011**, *353* (2), 512−518.
(43) Van der Waerden, B. L. Punkte Auf Der Kugel. Drei Zusatze. *Math. Ann.* **1952**, *125* (1), 213−222.
(44) Balmer, J. A.; Armes, S. P.; Fowler, P. W.; Tarnai, T.; Gaspar, Z.; Murray, K. A.; Williams, N. S. J. Packing Efficiency of Small Silica Particles on Large Latex Particles: A Facile Route to Colloidal Nanocomposites. *Langmuir* **2009**, *25* (9), 5339−5347.
(45) Quickenden, T. I.; Tan, G. K. Random Packing in Two Dimensions and the Structure of Monolayers. *J. Colloid Interface Sci.* **1974**, *48* (3), 382−393.
(46) Dinsmore, A. D.; Hsu, M. F.; Nikolaides, M. G.; Marquez, M.; Bausch, A. R.; Weitz, D. A. Colloidosomes: Selectively Permeable Capsules Composed of Colloidal Particles. *Science* **2002**, *298* (5595), 1006−1009.
(47) Bausch, A. R.; Bowick, M. J.; Cacciuto, A.; Dinsmore, A. D.; Hsu, M. F.; Nelson, D. R.; Nikolaides, M. G.; Travesset, A.; Weitz, D. A. Grain Boundary Scars and Spherical Crystallography. *Science* **2003**, *299* (5613), 1716−1718.
(48) Gonzenbach, U. T.; Studart, A. R.; Tervoort, E.; Gauckler, L. J. Ultrastable Particle-Stabilized Foams. *Angew. Chem., Int. Ed.* **2006**, *45* (21), 3526−3530.
(49) Datta, S. S.; Gerrard, D. D.; Rhodes, T. S.; Mason, T. G.; Weitz, D. A. Rheology of Attractive Emulsions. *Phys. Rev. E - Stat. Nonlinear, Soft Matter Phys.* **2011**, *84* (4), 3−8.
(50) Lewis, J. A. Colloidal Processing of Ceramics. *J. Am. Ceram. Soc.* **2000**, *83* (10), 2341−2359.
(51) Hermes, M.; Dijkstra, M. Jamming of Polydisperse Hard Spheres: The Effect of Kinetic Arrest. *Europhys. Lett.* **2010**, *89* (3), 38005.

DOI: 10.1021/acs.langmuir.7b01476
Langmuir XXXX, XXX, XXX−XXX